PAPER

Experimental study of flute instability by even/odd-parity quadrupole fields in Keda Mirror with AXisymmetricity (KMAX)

IOP Publishing Plasma Physics and Controlled Fusion
Plasma Phys. Control. Fusion **67** (2025) 035017 (11pp) https://doi.org/10.1088/1361-6587/adb3cc

Experimental study of flute instability by even/odd-parity quadrupole fields in Keda Mirror with AXisymmetricity (KMAX)

Qing Li[1], Xiaotian Teng[1], Weijian Qin[1], Zelin Xu[1], Jiacheng Ying[1], Yutao Chen[1], Yichi Zhang[1], Yilin Li[1], Jingran Wen[1], Zhida Yang[1], Ming Liu[2], Baoming Ren[2] and Xuan Sun[1,2,*]

[1] Department of Plasma Physics and Fusion Engineering, University of Science and Technology of China, Hefei, Anhui 230026, People's Republic of China
[2] Xeonova. Ltd, Hefei, Anhui 230026, People's Republic of China

E-mail: xsun@ustc.edu.cn

Received 19 November 2024, revised 11 January 2025
Accepted for publication 7 February 2025
Published 20 February 2025

Abstract

This study investigates the stabilization of flute mode instabilities in the Keda Mirror with AXisymmetry device, specifically focusing on the $m = 1$ mode that propagates in the direction of electron diamagnetism due to the $\boldsymbol{E} \times \boldsymbol{B}$ force. To mitigate this instability, quadrupole field (QPF) antennas were designed with either even or odd parity, depending on the direction of the induced current. Experimental results reveal that even parity significantly enhances stability, reducing fluctuation values at the plasma boundary by approximately 50%, while odd parity achieves only a 10% to 20% reduction. Radial particle flux measurements indicate a decrease to one-tenth of the original value when the even-parity QPF is applied during the wash-gun injection phase, with no correlation observed between ion saturation current and angular electric field fluctuations. The stability enhancement is attributed to the positive magnetic pressure gradient generated by the QPF. Further analysis incorporating magnetic field curvature reveals that the beneficial effects are more pronounced with even parity. However, the density measured by the interferometer decreases significantly with increasing even-parity QPF current, while the density with odd parity remains largely unchanged.

Keywords: axisymmetric tandem mirror, flute instability, quadrupole field, magnetic field curvature

1. Introduction

Recent advancements in magnetic mirror research have significantly enhanced our understanding of magnetic confinement systems. Notable modern configurations, including the Wisconsin HST Axisymmetric Mirror (WHAM) [1, 2], the Break Even Axisymmetric Mirror (BEAM) [3], the Centrifugal Mirror Fusion Experiment (CMFE) [4, 5], and the Novatron, each present unique approaches to improving confinement and stability, thereby shaping the evolving landscape of magnetic mirror technology.

These advanced magnetic mirrors are predominantly axisymmetric devices [6–9]. The axisymmetric mirror configuration offers several advantages: (1) its simple engineering structure facilitates maintenance and upgrades; (2) the axisymmetric design mitigates neoclassical and resonant transport [10], thereby enhancing radial confinement; (3) breakthroughs

* Author to whom any correspondence should be addressed.

in high-temperature superconducting materials [11] have enabled the development of axisymmetric devices with high magnetic mirror ratios, significantly improving axial confinement of plasma particles. A notable example is the medium-sized axisymmetric mirror, the gas-dynamic trap (GDT) [12, 13] at the Budker Institute in Novosibirsk, Russia. Recently, the GDT has been equipped with a 0.7 MW/54.5 GHz electron cyclotron resonance heating system and a 5 MW neutral beam injection system, achieving electron temperatures near 1 keV and a plasma β (the ratio of plasma pressure to magnetic pressure) of approximately 60% [14]. This breakthrough demonstrates the potential for high-β plasma confinement and marks a significant step forward in advancing axisymmetric magnetic mirrors toward practical fusion reactors.

However, a key challenge in magnetic mirror systems is the flute mode instability, which can severely degrade confinement and system efficiency due to macroscopically propelling the plasma to the walls. Ryutov *et al* has cataloged various stabilization methods for flute mode [15], although many of these rely heavily on altering the magnetic field line configuration—such as cusp-field or divertor stabilization [16–20]. These methods tend to be ineffective when the plasma β becomes sufficiently large, as the magnetic field lines lose their rigidity [21]. The GDT, for example, achieves a high β by utilizing vortex confinement [22], which is induced by the application of biased electrodes. WHAM, a high-field platform for prototyping fusion technologies, may also employ shear-flow stabilization techniques to mitigate interchange modes. However, the electrode configuration in the device can lead to sputtering, which cools the plasma and complicates its performance. Another problem is that in a mirror machine with well-confined plasma, the coupling to the end cells should be poor and the ability to generate strong shear will be diminished. For this reason, it is questionable whether vortex confinement is applicable in long, tandem mirror machine. To address this, Igor Kotelnikov [23] proposed a wall-stabilization method for WHAM, in which a lateral wall is installed around the plasma column, and a current is driven opposite to the diamagnetic current through the wall. This approach can stabilize not only the flute mode but also ballooning instabilities [24]. However, simulation results suggest that the critical β for stability is highly dependent on the radial profile of the plasma column and the gap between the plasma column and the lateral wall, which may cause problems in practice.

The multipole field is similar to the Ioffe rods [25], which was originally used in a simple magnetic mirror to suppress flute instability. This concept was later adapted for use in the anchor cells of tandem magnetic mirrors, evolving into the baseball coil configuration, and later into Yin-Yang coils [26]. Multipole fields are also employed in field-reversed configurations (FRCs) to stabilize $n = 2$ rotational instabilities [27] and $n = 1$ wobble motion [28] by magnetic pressure. Additionally, multipole fields are commonly used in tokamaks to correct local magnetic field errors and mitigate resistive wall modes [29].

Rotating magnetic fields (RMFs) have been demonstrated to effectively control the $n = 2$ rotational instability in FRC plasmas [30]. The parity of the RMF is distinguished by whether the axial antenna currents on both sides of the midplane are aligned in the same direction or reversed. Guo *et al* showed that RMF parity plays a crucial role in influencing both plasma stability and energy confinement [31]. In particular, the odd-parity RMF configuration significantly enhances stability and improves energy confinement. Additionally, Cohen and Milroy [32] demonstrated that the odd-parity configuration favors the closure of FRC magnetic field lines, a finding that was corroborated by Milroy's simulations [33]. In experiments, it was observed that using an odd-parity RMF antenna produced a plasma with an electron temperature of approximately 200 eV [34], while an electron temperature of only 50 eV was achieved under even-parity conditions [35]. Moreover, rapid ion heating was observed when the frequency of the odd-parity RMF was within the ion cyclotron range [36].

In this study, we investigate the stabilizing effects of quadrupole fields (QPFs) on flute mode in *a* axisymmetric tandem magnetic mirror. Two sets of QPF coils are strategically placed in the central chamber to examine their influence on flute mode stabilization. These coils are configured to produce either even or odd parity, based on the direction of the current. When the axial current directions of the two antenna sets are in the same direction, the configuration is considered to have even parity; otherwise, it is classified as odd parity. The utilization of multipole fields offers several advantages, including a simplified structural design, external placement relative to the vacuum chamber, and the elimination of issues such as sputtering. Consequently, the QPF configuration enhances the stability of the magnetic mirror while also ensuring ease of integration and operation.

This study aims to explore innovative methods for stabilizing flute mode instabilities using QPFs with varying parity. By investigating these advancements, we seek to demonstrate the potential of this technique in improving magnetic mirror performance and advancing the field of plasma confinement. Furthermore, we hope that the findings of this work will contribute to the stabilization of MHD modes in some stellarators, such as TJ-II, which rely on magnetic well for confinement [37, 38].

2. Experiment setup

The experiments described herein are conducted using the KMAX (Keda Mirror with AXisymmetry) device, which consists of a central chamber, two end cells, and two expanders. A longitudinal magnetic field, stable over time relative to plasma lifetime, is generated by 16 axially distributed solenoids powered by eight independent modules. The longitudinal field distribution along the system axis is illustrated in figure 1(b). The base pressure within the device is maintained at approximately 10^{-4} Pa, facilitated by the use of three molecular pumps, while the operating pressure for hydrogen is typically (2–5) $\times$ 10^{-2} Pa.

Figure 1(a) outlines the diagnostics employed in this study. The rake probe, designed as a triple probe array, diagnoses

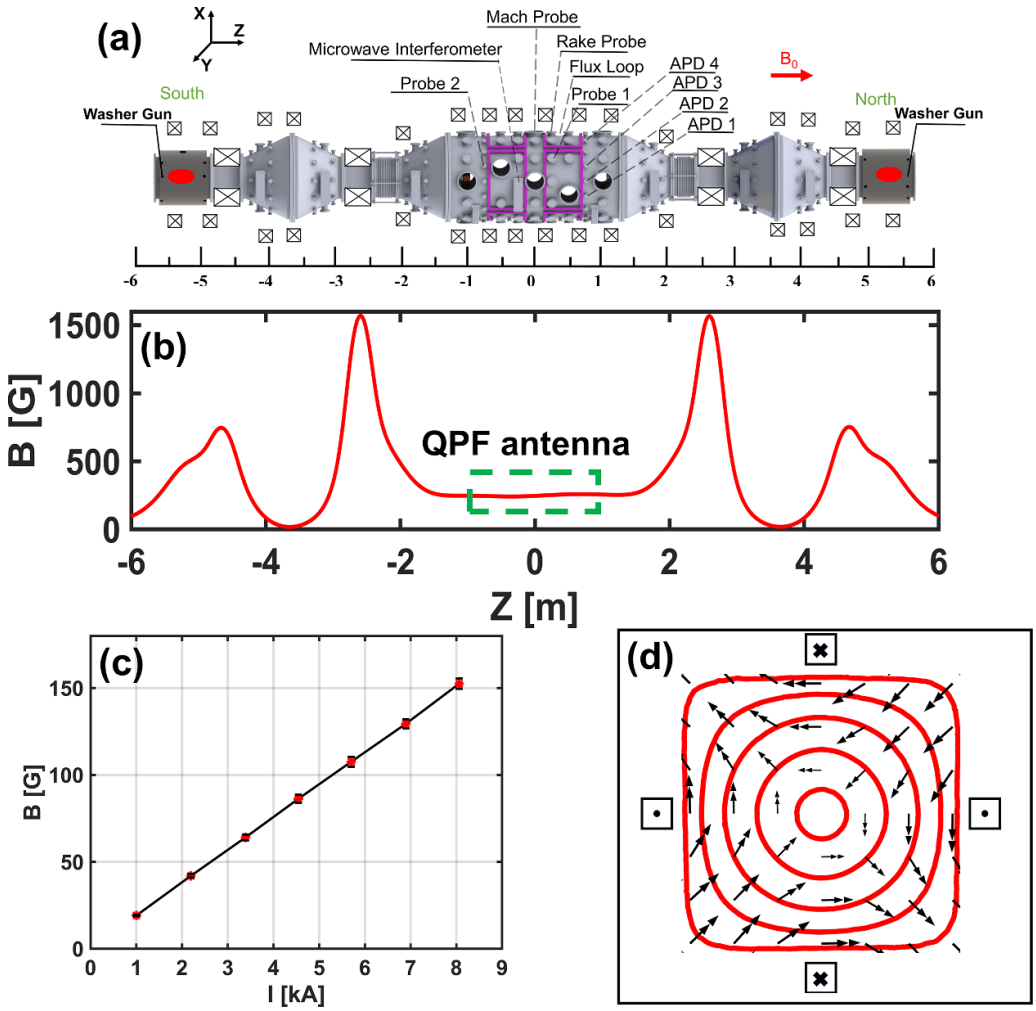

Figure 1. (a) Schematic drawing of KMAX with the QPF antenna and diagnostics. The purple coil in the center cell is where the quadrupole antennas are located. (b) Profile of magnetic flux density on the axis. The green rectangular box delineates the extent of the quadrupole field, which ranges approximately from -0.75 m to 0.75 m. (c) The magnetic field strength at the geometric center of the quadrupole field coil under different current. (d) Contour of the quadrupole field antenna mid-plane.

the radial plasma density profile and fluctuations in ion saturation currents. Probes 1 measures the radial flux [39], defined as $\Gamma_r = \langle \tilde{N}_e \cdot \tilde{v_e} \rangle = \langle \tilde{N}_e \cdot \tilde{E}_\theta \rangle / B_0 \propto \langle \tilde{I}_{sat} \cdot \tilde{E}_\theta \rangle / B_0$, where $\tilde{N}_e$ is fluctuating density estimated from fluctuating ion saturation current $\tilde{I}_{sat}$, $\tilde{E}_\theta$ is angular fluctuating electric field derived from floating potential measurements, $\tilde{v_e}$ is fluctuating radial velocity and B_0 is DC field strength. An interferometer located at $z = -0.3$ m measures the plasma line-integrated density. Four avalanche photodiodes (APDs) are positioned at $z = 0.75$ m at angles of $-40°$, $-20°$, $0°$, and $80°$ to assist in identifying flute instability through light emission measurements [40].

The QPF coils are situated in the gap between the primary longitudinal coil and the central cell wall, as indicated by the purple coils in figure 1(a). Each coil frame comprises ten turns of thin copper sheet with a rectangular cross-section of 0.5×40 mm, totaling eight frames, with layers insulated by polyimide film. These coils are powered by four 150 V, 60 F supercapacitors, achieving a single-turn current of up to 1 kA. Current switching to the coils is facilitated by insulated gate bipolar transistors, with a current plateau duration reaching up to 20 ms. The magnetic diffusion time for the QPF to pass through the 1 cm thick stainless steel wall of the device is approximately 200 μs. A Hall-effect sensor measures the magnetic field strength produced by the QPF coil at the geometric center of each coil, with results displayed in figure 1(c). Although the coils differ slightly, the variation is controlled within 7%, satisfying experimental requirements. Figure 1(d) depicts the isoline map of the magnetic field in the central plane of the coil, revealing uniformity in the radial direction at smaller radii, which diminishes as proximity to the wall increases.

The hydrogen plasma is produced by washer-guns mounted on endplates of the device [41]. Typical electron density, temperature and floating potential at $z = 0.4$ m are displayed in figure 2, measured by Probe 1. The radial profile of the plasma density follows a near-parabolic distribution, while the electron temperature remains nearly constant across the radial direction, dropping sharply near the plasma edge.

The QPF configuration is categorized based on the current directions of adjacent coils along the z-axis into even parity

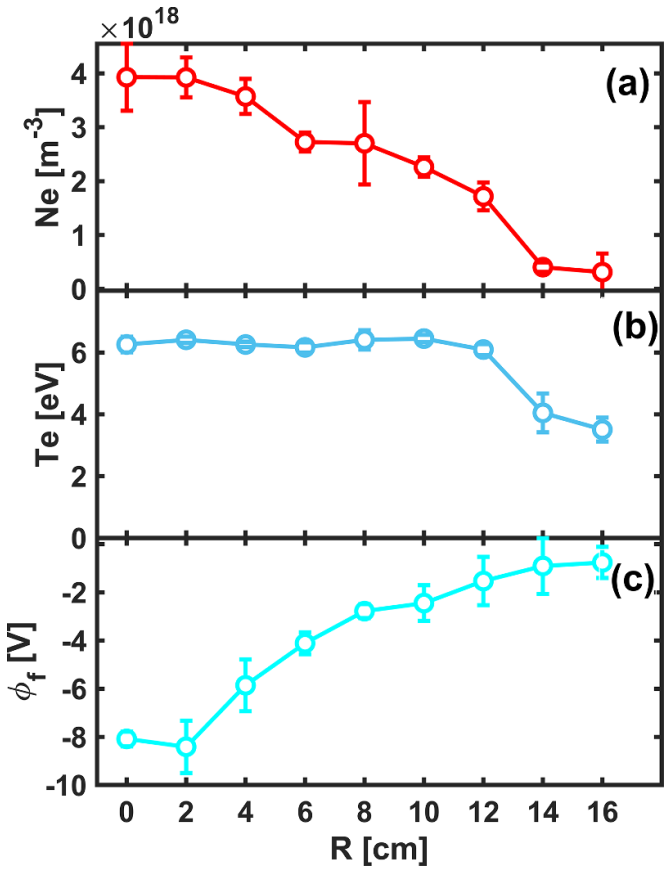

Figure 2. Typical profile of (a) electron density, (b) electron temperature and (c) floating potential.

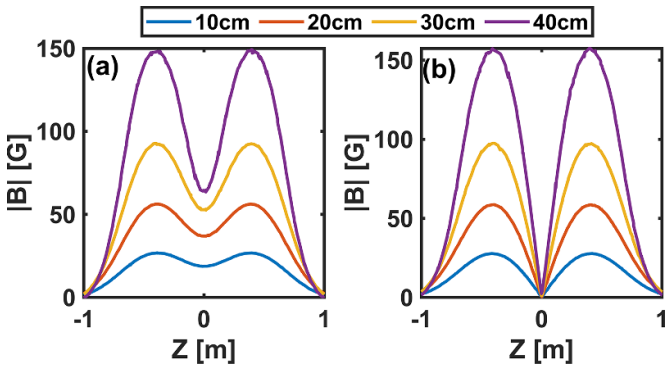

Figure 3. Profile of quadrupole magnetic field amplitude in y–z plane with (a) even parity and (b) odd parity.

and odd parity. When the magnetic field directions of two adjacent coils are aligned, they exhibit even parity; conversely, if they oppose each other, they represent odd parity. Figure 3 illustrates the profile of the quadrupole magnetic field (QPF) amplitude in the y–z plane, with varying colors indicating different radial positions, derived from a simulation with a total current of 10 kA. Note that figure 3 is pure QPF, without superimposing the background mirror magnetic field. Notably, the magnetic field strength in the odd-parity configuration remains consistently zero across the plane.

The non-axisymmetric nature of the QPF leads to a disruption of the axisymmetry in the original mirror field configuration. Figure 4 presents the magnetic field line profiles in the x–z and y–z planes after superimposing the background mirror field with the QPF. The mirror field strength corresponds to that shown in figure 1(b), while the QPF current is set to 6 kA. To better highlight the effects of field line deformation, despite the actual plasma radius at $z = -2$ m being approximately 10 cm, the magnetic field lines are drawn starting from a radius of 50 cm to emphasize the variations in field topology.

From figure 4, it is evident that the QPF causes a rearrangement of the magnetic field line distribution. In the even-parity case, where the magnetic fields of the two adjacent coils are aligned, the magnetic field lines experience continuous variations. In contrast, in the odd-parity configuration, where the magnetic fields of the two coils along the axial direction are oppositely aligned, the second coil partially 'corrects' the deformation induced by the first coil. For instance, in the x–z plane, the magnetic field generated by the first quadrupole coil causes a divergence effect in the magnetic field lines, while the second coil induces a convergence effect. As a result, the deformation of the field lines is less pronounced in the odd-parity case compared to the even-parity QPF.

3. Experimental results

3.1. Identification of the instability

In linear magnetized plasma devices, three primary types of instability are typically observed: diamagnetic drift waves, Rayleigh–Taylor (RT) instability due to curvature, and Kelvin–Helmholtz (K–H) shear flow instability. Given that this experiment lacks a velocity shear mechanism, K–H instability is not considered. The characteristics of these instabilities have been summarized by Jassby [42], as detailed in table 1, which aids in identifying the type of instability present in this experiment.

Figure 5(a) displays the fluctuation signals from the APDs positioned at the same axial location but different angular positions. The observed phase differences among the four APDs indicate a mode of $m = 1$, consistent with previous findings [19]. The radial electric field points inward, and the floating potential in figure 2(c) supports this observation. The APD measurements indicate that the fluctuations propagate in the direction of electron diamagnetism, caused by the $Er \times Bz$ force. When APD 1 is relocated to $z = -0.75$ m to match the angular position of APD 2, minimal phase difference is observed. And previous datas [43] indicate that the parallel wave number $k_{||} \approx 0$, with an error of approximately $3\% \times 2\pi/L$, where L is the distance between the two mirrors. A crucial characteristic of drift waves is their propagation, which includes axial and angular components, thereby confirming that the observed instability is not a drift wave.

The instability is most pronounced at $r = 12$ cm, as indicated by the rake probe measurements. Figure 6(a) illustrates the term $|n^{-1}(\partial n/\partial r)|$ as a function of radial position, suggesting the presence of RT instability according to table 1. The

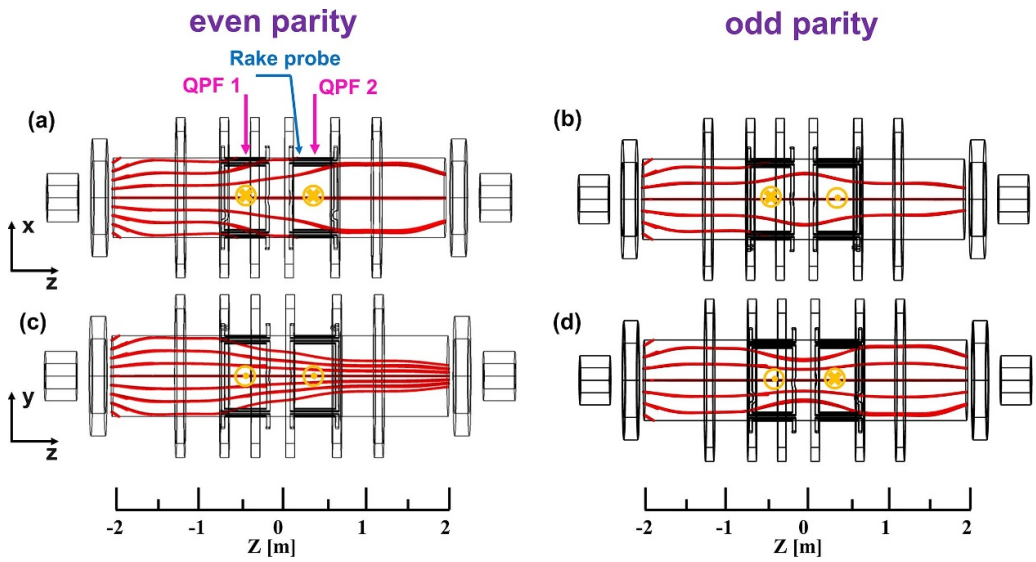

Figure 4. Cross-sectional view of magnetic field lines resulting from the superposition of a quadrupole field onto a background mirror field. Subgraphs (a) and (c) show the magnetic field line profiles in the x–z and y–z planes with even parity, respectively, while subgraphs (b) and (d) display the profiles with odd parity. The red streamlines in the figure represent magnetic field lines, the blue arrow indicates the rake probe position, the pink arrow marks the locations of the two quadrupole field groups, and the yellow symbol represents the direction of the magnetic field from the saddle-shaped coil at that location.

Table 1. Criteria for the characterization of drift waves, Rayleigh–Taylor and Kelvin–Helmholtz instabilities [42].

Property	Drift wave	Rayleigh–Taylor	Kevin–Helmholtz
Radial location	Max $\omega_{E\times B}$	Max$\left\|n^{-1}\left(\partial n/\partial r\right)\right\|$	Maximum of the velocity shear
$\kappa_{\parallel}$	$\sim 1/L$	0	0
Max$\left(e\tilde{\phi}/k_{\mathrm{B}}T_{\mathrm{e}}\right)$	1	1	$\gg 1$
Max$\left(\frac{e\tilde{\phi}}{k_{\mathrm{B}}T_{\mathrm{e}}}/\frac{\tilde{n}}{n}\right)$	$\leqslant 1$	$\geqslant 1$	$\gg 1$

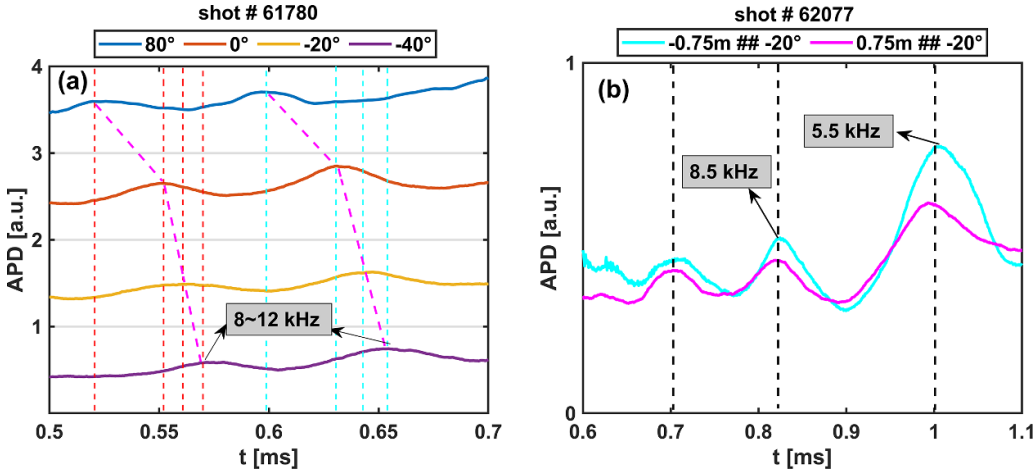

Figure 5. Fluctuations measured by APDs (a) at different azimuthal and (b) at different axial positions.

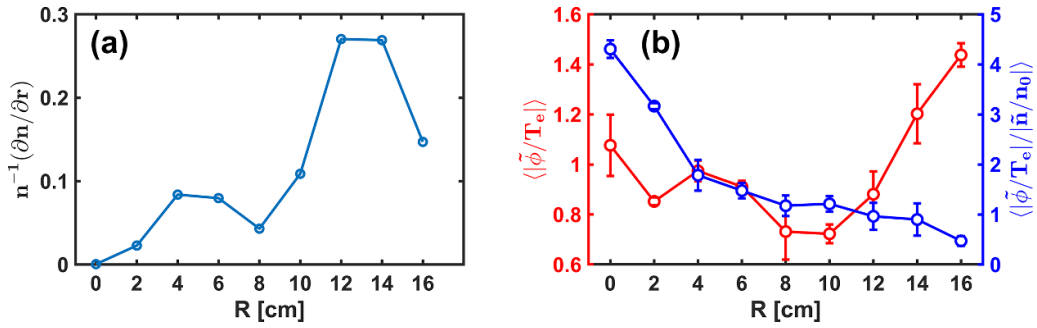

Figure 6. (a) Profile of density scale length $n^{-1}(\partial n/\partial r)$, (b) red curve: relative amplitude of potential fluctuations. Blue curve: ratio between the potential and the density fluctuations.

ratios $\langle|\frac{e\tilde{\phi}}{k_B}T_e|\rangle$ and $\langle|\frac{e\tilde{\phi}}{k_B T_e}/\frac{\tilde{n}}{n}|\rangle$ show a significantly greater than 1 for K–H instability. As depicted in figure 6(b), at $r = 12$ cm, $\langle|\frac{e\tilde{\phi}}{k_B T_e}|\rangle \approx 0.9$, $\langle|\frac{e\tilde{\phi}}{k_B T_e}/\frac{\tilde{n}}{n}|\rangle \approx 1$. The amplitudes of the density and potential fluctuations align well with expectations for RT instability. Consequently, we conclude that the observed instability is indeed RT instability rather than a drift wave or K–H instability.

3.2. QPF stabilization

Flute instability, also known as magnetic Rayleigh–Taylor instability, arises because the centrifugal force experienced by particles in a magnetic field acts analogously to gravity. In this context, the finite Larmor radius (FLR) effect is generally not significant for the stabilization of the $m = 1$ flute mode in mirror magnetic fields, except when a conducting wall is positioned close to the plasma surface [44]. This effect has been experimentally confirmed in the GDT [45]. To stabilize the flute mode with $m > 1$, the magnetic mirror must either be sufficiently long or the ion gyroradius must be large enough to satisfy the condition [15]

$$m > 2\frac{a^2}{L\rho_i} = 2\frac{a/\rho_i}{L/a} \tag{1}$$

where a is plasma radius, L is mirror-mirror length, is ion gyroradius. In KMAX device, $\rho_i \sim 6$ mm, $L \sim 5$ m, and $a \sim 15$ cm. With $a/\rho_i \sim 26$ and $L/a \sim 33$, it follows that the flute mode with $m > 1$ should be effectively stabilized by FLR effect.

As previously mentioned, the two sets of QPF antennas are classed into even parity and odd parity based on their current directions. Our experiments demonstrate that even parity yields superior stabilization, a topic that will be explored further. Figure 7 presents raw data and frequency spectra from the rake probe with even parity, focusing on $r = 12$ cm and $r = 16$ cm—the regions most susceptible to flute mode instability. Without the QPF current, the plasma in the outer layers exhibits significant instability characterized by large low-frequency perturbations, with frequencies ranging from 5 to 30 kHz and a peak spectral intensity near 10 kHz (see figures 7(1-b) and (2-b)). The perturbation frequency of the ion saturation current gradually decreases over time, and it appears to vanish completely after approximately 1 ms. We hypothesize that this is due to the accumulation of neutral gas, which increases collisions and viscous forces with the plasma, thereby dissipating the free energy associated with the instability and contributing to the stabilization of the plasma. When the QPF current is increased to 2.4 kA, these perturbations are substantially mitigated, with the frequency domain amplitude decreasing to less than half. Further increases in current lead to nearly complete disturbance suppression, although a corresponding decrease in ion saturation flow is observed when comparing figures 7(1-a) and (1-g).

Figure 8 illustrates the fluctuation levels of ion saturation currents as a function of QPF current for both even and odd parity configurations. The fluctuation value is given by $\tilde{I}_{sat} = \sqrt{\frac{1}{N}\sum_{i=1}^{N}\left(\frac{x_i-\bar{x}}{\bar{x}}\right)^2}$, where N is the number of data, $\bar{x}$ is the average value of ion saturation current, shown as black lines in figure 7.

Notably, a significant reduction in plasma fluctuations is observed at 2.4 kA with even parity, where fluctuation values are approximately halved compared to conditions without QPF. As the even-parity current increases beyond 2.4 kA, the fluctuation values remain relatively constant. In contrast, the reduction in fluctuation for odd parity is approximately 20% at $r = 12$ cm and 10% at $r = 16$ cm.

The radial flux of particles is closely related to fluctuations in ion saturation current and angular electric field, which are calculated by subtracting the moving average from the corresponding raw data measured using a four-pin Langmuir probe (Probe 1). The left column of figure 9 depicts the data without the QPF, while the right column displays results with a current of 4.8 kA. The radial flux was measured at $r = 12$ cm, where the instability was most pronounced. According to figure 7, the instability primarily occurs between 300 μs and 1.2 ms. During this period, we measured the radial particle flux. The application of the QPF leads to significant suppression of fluctuations in both ion saturation current and angular electric field. Figures 9(e) and (f) illustrate the time evolution of fluctuation-induced particle flux. In the absence of the QPF, the radial flux is positive, indicating outward particle loss. However, with the QPF applied, this value decreases to one-tenth, and $\tilde{I}_{sat}$ and $\tilde{E}_\theta$ lose coherence, as shown in

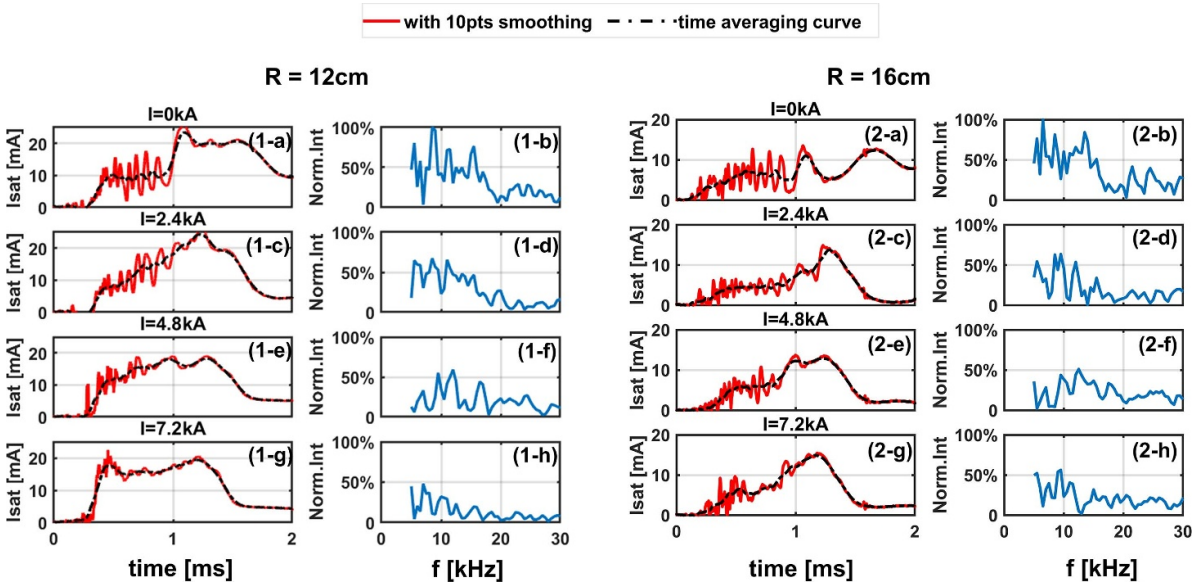

Figure 7. Comparison of plasma with different quadrupole field current. The figures in first column and third column are the ion saturation currents collected by rake probes at $r = 12$ cm and 16 cm, respectively, with the black dash-dotted lines as the average values, and the figures in the second and fourth column are fluctuation in frequency domain.

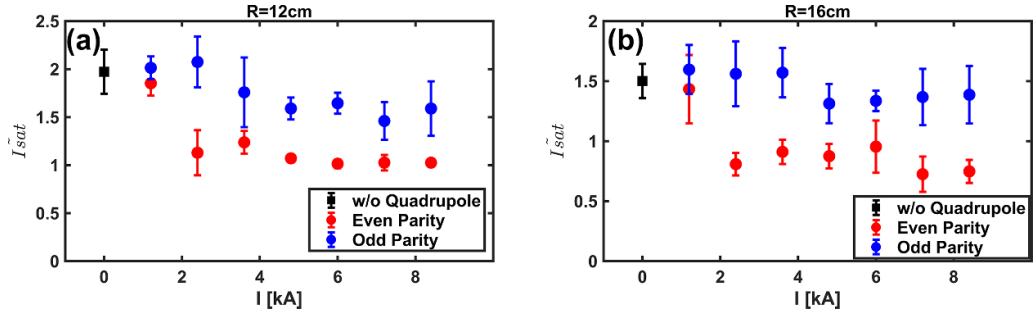

Figure 8. Measured fluctuations as functions of the QPF current with even parity and odd parity at (a) $r = 12$ cm and (b) $r = 16$ cm. The error bar represents the mean square error of repeated experiments.

figures 9(g) and (h). The cross-coherence is defined as [39]:

$$\gamma_{(\tilde{I}_{\rm sat},\tilde{E}_\theta)} = \sqrt{\frac{\left|P_{(\tilde{I}_{\rm sat},\tilde{E}_\theta)}\right|^2}{P_{(\tilde{I}_{\rm sat})}P_{(\tilde{E}_\theta)}}}. \tag{2}$$

Here, $P_{(\tilde{I}_{\rm sat})}$ and $P_{(\tilde{E}_\theta)}$ denote the power spectra of $\tilde{I}_{\rm sat}$ and $\tilde{E}_\theta$, respectively. $P_{(\tilde{I}_{\rm sat},\tilde{E}_\theta)}$ is the cross-power of $\tilde{I}_{\rm sat}$ and $\tilde{E}_\theta$. These quantities are transformed into the frequency domain.

To understand why even parity stabilizes more effectively than odd parity, we can analyze the field pressure gradient. In the mid-plane of the antenna, the magnetic field intensity generated by the QPF increases almost linearly in the radial direction until it approaches the plasma boundary. This behavior aligns with theoretical predictions, where the multipole field near the axis is approximately described by [46],

$$B = \frac{\mu_0 m I_m}{\pi r_m}\left(\frac{r}{r_m}\right)^{m-1}. \tag{3}$$

Here, r_m, 2 m, μ_0 represent the radial position of the coil, the order of the multipole field, and the permeability of free space, respectively. Setting $m = 2$ for the QPF results in a field strength that is linear with respect to the radial position. Figure 10 shows the comparison of magnetic field gradients with even parity and odd parity. Notably, the odd-parity antenna does not generate a strong positive magnetic field gradient in the mid-plane, even nearing zero. This lack of gradient may contribute to the reduced stability of the flute mode, as suggested by Taylor's theory [47].

3.3. Curvature effect

The superposition of the QPF on the background magnetic field significantly influences the overall field line structure. This interaction disrupts the axial symmetry of the original magnetic field and alters the curvature of the magnetic lines. Figure 11 illustrates the distortion of magnetic field lines when a 6 kA QPF current is applied. Panels (a) and (b) show the magnetic field lines in the x–z and y–z planes with even parity, respectively, while panels (c) and (d) display the magnetic

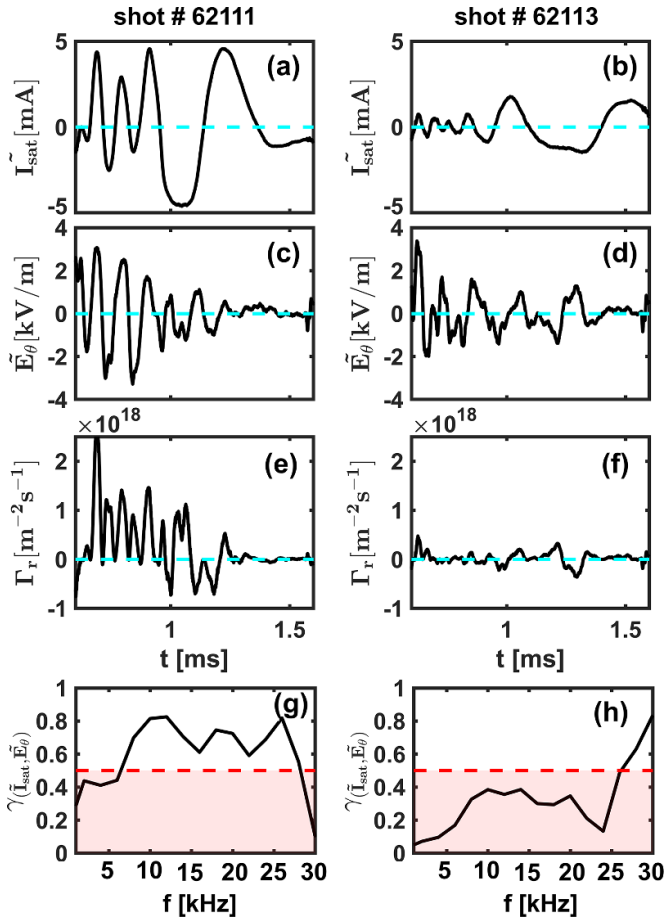

Figure 9. Comparison of the plasma with the QPF off (shot No. 62111, left column) and on (shot No. 62113, right column) at $r = 12$ cm. Time evolutions of [(a) and (b)] the fluctuations of the angular electric fields, $\tilde{E}_\theta$ and [(c) and (d)] the fluctuations of the ion saturation current, $\tilde{I}_{\rm sat}$. Figures (e) and (f) are the radial particle flux. Figures (g) and (h) are coherence $\gamma_{(\tilde{I}_{\rm sat},\tilde{E}_\theta)}$.

field lines in the x–z and y–z planes with odd parity. The starting point of the magnetic field lines is located at $z = -2$ m, $r = 0.1$ m. The magnetic field lines from this starting point have an approximate radius of 15 cm in the midplane, which corresponds to the plasma radius. The red and blue arrows indicate regions of good and bad curvature, where the good curvature refers to the curvature that bends toward the plasma. As shown in figure 11, the even-parity case exhibits a greater concentration of good curvature, which is favorable for plasma confinement.

To quantify the expression, we calculate the pressure-weighted curvature criterion as derived by Rosenbluth and Longmire [48]:

$$\int \frac{(p_\parallel + p_\perp)\,\kappa}{rB^2}{\rm d}l \geqslant 0 \tag{4}$$

where κ is the curvature of the magnetic field lines, r is the distance of the magnetic field line from the axis. $p_\parallel$ and $p_\perp$ are the parallel and perpendicular plasma pressure, respectively. For simplicity, we assume that the pressure terms are constant along the magnetic field lines. Next, we integrate the curvature

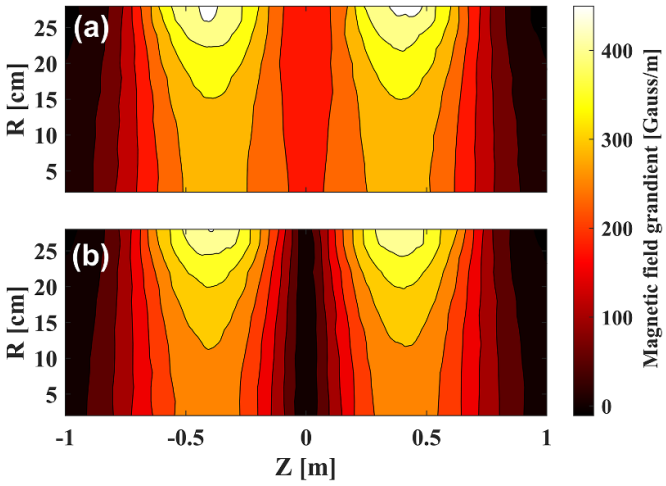

Figure 10. Comparison of magnetic field gradients with (a) even parity and (b) odd parity.

over the central chamber, with the integration bounds for the distance z ranging from -2 m to $+2$ m:

$$I_{\rm c} = \int \frac{\kappa}{rB^2}{\rm d}l. \tag{5}$$

Figure 12 shows the evolution of curvature integral with quadrupole field current with even and odd parity. Due to the presence of the magnetic throat, the integral of the overall curvature of the central cell is consistently negative. However, when a QPF current is applied, the integral value increases, regardless of whether even or odd parity is used. Notably, the integral value increases more rapidly with even parity, particularly after reaching a current of 2 kA. This trend is in good agreement with the results shown in figure 8. When the current increases from 7 kA to 8 kA, a sharp rise in the integral value is observed with even parity. This sudden increase occurs because, at this current level, some of the magnetic field lines undergo significant deformation, which causes them to come into close contact with the device wall.

Figure 13 illustrates the temporal evolution of the density measured by the interferometer with even and odd parity. With even parity, the density exhibits a clear decreasing trend as the QPF current increases. When the current reaches 6 kA, the density drops to nearly half of its value in the absence of current, especially after 1 ms, where the decrease becomes particularly significant. This could be due to the increased current redirecting the magnetic field lines toward the metal walls, leading to particle losses along the magnetic field lines. In contrast, no significant decrease in density is observed with odd parity. Furthermore, the enhanced stability with even parity is also evident. Specifically, between 0.5 ms and 1.2 ms, the fluctuation amplitude with even parity is significantly reduced, while with odd parity, fluctuation persists even at 6 kA, although it is lower compared to the fluctuation amplitude observed without QPF current.

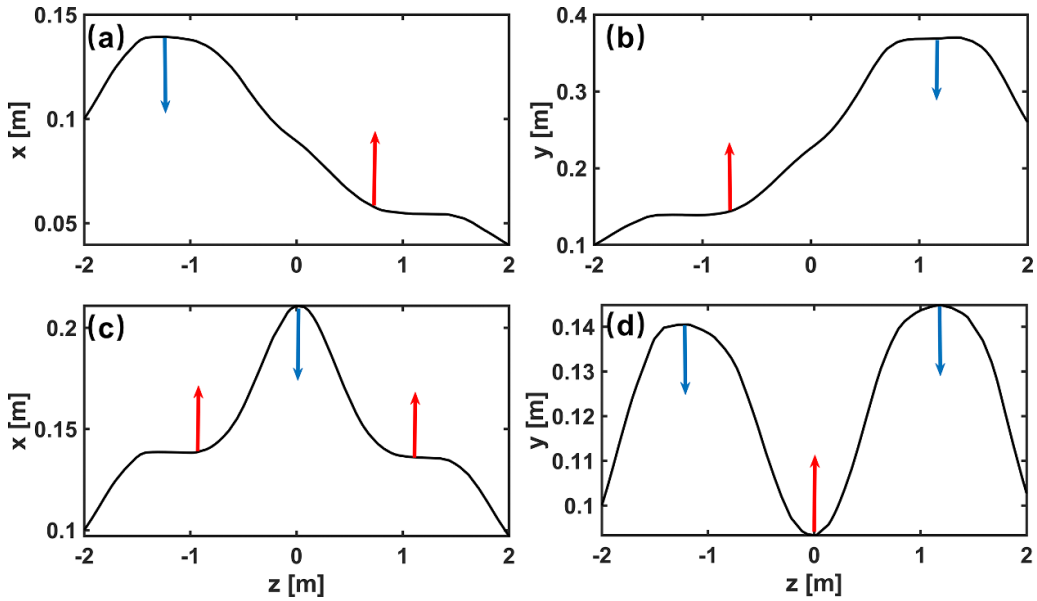

Figure 11. The magnetic field diagrams are based on a starting point at $z = -2$ m, and $r = 0.1$ m, with the following symmetry conditions: (a) and (b) exhibit even parity, while (c) and (d) exhibit odd parity. The diagrams are presented in two columns: the left column shows the x–z plane, and the right column shows the y–z plane.

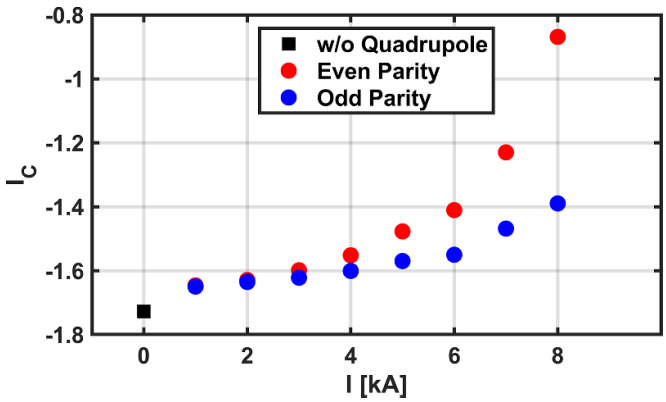

Figure 12. Evolution of curvature integral with quadrupole field current with even and odd parity.

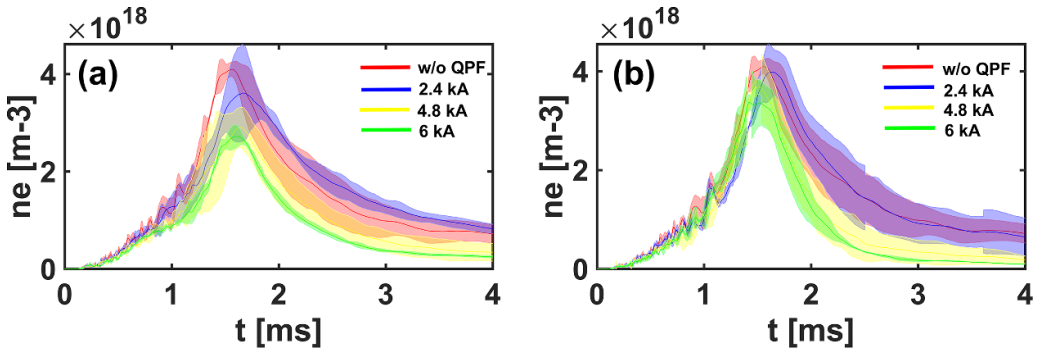

Figure 13. Temporal evolution of the density measured by the interferometer. Panels (a) and (b) correspond to even and odd parity, respectively. The width of the color band represents mean square error of repeated experiments.

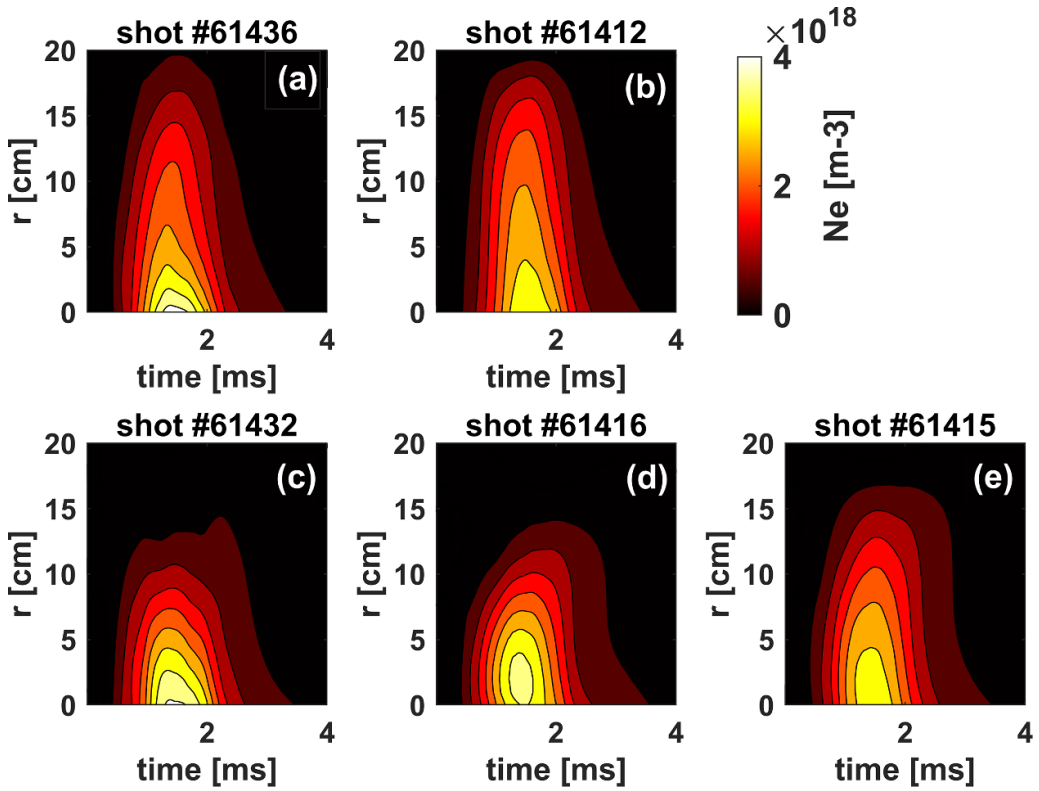

Figure 14. Comparison of plasma density profiles under different magnetic field configurations. The density profiles are measured by a rake probe. Panels (a), (b), (c), and (d) correspond to the magnetic field configurations in the subplots of figure 4, while panel (e) represents the case without the application of the quadrupole field. All panels share a common color bar.

Additionally, it is possible that the even-parity field drives the outer plasma-carrying field lines toward the wall, effectively short-circuiting the electric field. This mechanism could account for both the observed stabilization (due to wall coupling) and the reduction in plasma density.

To investigate the effect of the QPF on plasma distribution, plasma density radial profiles were measured using a rake probe, as shown in figure 14. In this experiment, the QPF current of 4.8 kA was applied. The experimental results demonstrate that the QPF significantly modifies the plasma profile, in agreement with the results presented in figure 4. Compared to the case without the QPF (figure 14(e)), larger plasma radii were observed under the magnetic configurations in panels (a) and (b) of figure 4, while smaller radii were measured in panels (c) and (d). These findings confirm the effective control of plasma shape by the QPF.

4. Conclusion

We have confirmed the presence of a flute mode with $m = 1$ in the KMAX device, propagating in the direction of electron diamagnetism due to the $\boldsymbol{E} \times \boldsymbol{B}$ force. To suppress this instability, we designed QPF antennas that can be classified into even and odd parity based on current direction. Measurements of ion saturation flow fluctuations from the rake probe indicate that even parity exhibits superior inhibition of this instability, with fluctuation values at the plasma boundary reduced by approximately 50%, while odd parity achieves only a 10% to 20% reduction.

Additionally, measurements of radial particle flux at the boundary reveal that, under the influence of the even-parity QPF, the flux decreases to one-tenth of its original value, and $\tilde{I}_{\mathrm{sat}}$ and $\tilde{E}_{\theta}$ show no correlation. The measurement result was obtained during the period of plasma instability. This indicates that the QPF stabilized the flute mode during this period and reduced the outward particle flux. The enhanced stability can be attributed to the magnetic pressure generated by the QPF, which establishes a positive magnetic pressure gradient. The efficacy of even parity over odd parity arises from the latter inability to produce an effective magnetic pressure gradient in the device's mid-plane. Subsequent analysis revealed that this result is also related to the magnetic field curvature and the electric field short-circuiting caused by the magnetic field lines leading to the wall.

Analysis of curvature integrals reveals that the integral value for even parity is higher than that for odd parity. However, as the current increases, the magnetic field lines in the even-parity case tend to shift toward the lateral wall, leading to a decrease in density, particularly after the plasma has been stabilized. In contrast, the density in the odd-parity case remains largely unchanged.

It is noteworthy that prior researchers had abandoned the use of QPF configurations due to concerns that they would disrupt the angular symmetry of the magnetic mirror. Our

experimental results demonstrate that effective stabilization of the flute mode can be achieved with as little as 2.4 kA of current (less than 5% of the longitudinal magnetic field), resulting in minimal disruption to the system's symmetry. However, as the strength of the QPF increases, the QPF helps with stabilization, but at the cost of reduced overall confinement. It offers new perspectives for future investigations into innovative magnetic confinement configurations, emphasizing the balance between achieving effective stability and improving confinement. Ultimately, these advancements hold promise for applications in advanced magnetic mirrors like WHAM, serving as a method for stabilizing plasma.

Data availability statement

All data that support the findings of this study are included within the article (and any supplementary files).

Acknowledgment

This work is supported by the Strategic Priority Research Program of the Chinese Academy of Sciences (Grant No. XDB0790303), and the National Natural Science Foundation under Grant No. 12175226.

ORCID iDs

Qing Li https://orcid.org/0009-0004-0845-1903
Xiaotian Teng https://orcid.org/0009-0000-5494-147X
Ming Liu https://orcid.org/0000-0002-2400-3017
Baoming Ren https://orcid.org/0000-0002-6443-3214
Xuan Sun https://orcid.org/0000-0002-8338-3654

References

[1] Endrizzi D *et al* 2023 *J. Plasma Phys.* **89** 975890501
[2] Egedal J, Endrizzi D, Forest C B and Fowler T K 2022 *Nucl. Fusion* **62** 126053
[3] Forest C B *et al* 2024 *J. Plasma Phys.* **90** 975900101
[4] Schwartz N R, Abel I G, Hassam A B, Kelly M and Romero-Talamás C A 2024 *J. Plasma Phys.* **90** 905900217
[5] Carson J and Sedwick R 2024 *Acta Astronaut.* **219** 438
[6] Post R F 2001 *Fusion Technol.* **39** 25
[7] Post R F 2003 *Fusion Sci. Technol.* **43** 195
[8] Post R F, Fowler T K, Bulmer R, Byers J, Hua D and Tung L 2005 *Fusion Sci. Technol.* **47** 49
[9] Fowler T K, Moir R W and Simonen T C 2017 *Nucl. Fusion* **57** 056014
[10] Cohen R H 1979 *Nucl. Fusion* **19** 1579
[11] Mitchell N *et al* 2021 *Supercond. Sci. Technol.* **34** 103001
[12] Ivanov A A and Prikhodko V V 2013 *Plasma Phys. Control. Fusion* **55** 063001
[13] Ivanov A A and Prikhodko V V 2017 *Phys.-Usp.* **60** 509
[14] Bagryansky P A, Shalashov A G, Gospodchikov E D, Lizunov A A, Maximov V V, Prikhodko V V, Soldatkina E I, Solomakhin A L and Yakovlev D V 2015 *Phys. Rev. Lett.* **114** 205001
[15] Ryutov D D, Berk H L, Cohen B I, Molvik A W and Simonen T C 2011 *Phys. Plasmas* **18** 092301
[16] Casey J A, Lane B G, Irby J H, Brau K L, Golovato S N, Guss W C, Kesner J, Post R S, Sevillano E and Zielinski J 1988 *Phys. Fluids* **31** 2009
[17] Ivanov A A *et al* 1994 *Phys. Plasmas* **1** 1529
[18] Katanuma I, Yagi K, Nakashima Y, Ichimura M and Imai T 2010 *Phys. Plasmas* **17** 032303
[19] Li Q, Zhu G, Ren B, Ying J, Yang Z and Sun X 2023 *Plasma Sci. Technol.* **25** 025102
[20] Kotelnikov I A, Ivanov A A, Yakovlev D V, Chen Z and Zeng Q 2020 *Nucl. Fusion* **60** 016008
[21] Beklemishev A D 2016 *Phys. Plasmas* **23** 082506
[22] Beklemishev A D, Bagryansky P A, Chaschin M S and Soldatkina E I 2010 *Fusion Sci. Technol.* **57** 351
[23] Kotelnikov I, Prikhodko V and Yakovlev D 2023 *Nucl. Fusion* **63** 066027
[24] Kotelnikov I, Zeng Q, Prikhodko V, Yakovlev D, Zhang K, Chen Z and Yu J 2022 *Nucl. Fusion* **62** 096025
[25] Ioffe M S and Sobolev R I 1964 *Sov. At. Energy* **17** 1112
[26] Damm C C 1984 *J. Vac. Sci. Technol.* A **2** 710
[27] Ohi S, Minato T, Kawakami Y, Tanjyo M, Okada S, Ito Y, Kako M, Gotô S, Ishimura T and Itô H 1983 *Phys. Rev. Lett.* **51** 1042
[28] Fujimoto K, Hoshikawa A, Ohmura S, Takahashi T, Nogi Y and Ohkuma Y 2002 *Phys. Plasmas* **9** 171
[29] Hender T C *et al* 2007 *Nucl. Fusion* **47** S128
[30] Guo H Y, Hoffman A L, Milroy R D, Miller K E and Votroubek G R 2005 *Phys. Rev. Lett.* **94** 185001
[31] Guo H Y, Hoffman A L and Steinhauer L C 2005 *Phys. Plasmas* **12** 062507
[32] Cohen S A and Milroy R D 2000 *Phys. Plasmas* **7** 2539
[33] Milroy R D, Kim C C and Sovinec C R 2010 *Phys. Plasmas* **17** 062502
[34] Cohen S A, Berlinger B, Brunkhorst C, Brooks A, Ferraro N, Lundberg D P, Roach A and Glasser A H 2007 *Phys. Rev. Lett.* **98** 145002
[35] Hoffman A L, Guo H Y, Miller K E and Milroy R D 2006 *Phys. Plasmas* **13** 012507
[36] Cohen S A and Glasser A H 2000 *Phys. Rev. Lett.* **85** 5114
[37] Castellano J, Jiménez J A, Hidalgo C, Pedrosa M A, Fraguas A L, Pastor I, Herranz J, Alejaldre C and Team T-I 2002 *Phys. Plasmas* **9** 713
[38] de Aguilera A M *et al* 2015 *Nucl. Fusion* **55** 113014
[39] Powers E J 1974 *Nucl. Fusion* **14** 749
[40] Moon C *et al* 2021 *Sci. Rep.* **11** 3720
[41] Yi H, Liu M, Shi P, Yang Z, Zhu G, Lu Q and Sun X 2018 *Rev. Sci. Instrum.* **89** 043503
[42] Jassby D L 1972 *Phys. Fluids* **15** 1590
[43] Zhu G, Shi P, Yang Z, Zheng J, Luo M, Ying J and Sun X 2019 *Phys. Plasmas* **26** 042107
[44] Rosenbluth M N, Krall N A and Rostoker N 1962 *Nucl. Fusion Suppl.* **1** 143–50
[45] Anikeev A V, Bagryansky P A, Ivanov A A, Kuzmin S V and Salikova T V 1992 *Plasma Phys. Control. Fusion* **34** 1185
[46] Taylor J B 1963 *Phys. Fluids* **6** 1529
[47] Taylor J B 1964 *Phys. Fluids* **7** 767
[48] Rosenbluth M N and Longmire C L 1957 *Ann. Phys.* **1** 120